

LETTER • OPEN ACCESS

Maximisation of synchronisability under low injection power


To cite this article: Hisa-Aki Tanaka *et al* 2024 *EPL* **146** 52001

View the [article online](#) for updates and enhancements.

You may also like

- [Competing role of interactions in synchronisation of exciton–polariton condensates](#)
Saeed A Khan and Hakan E Türeci
- [Quantum synchronisation enabled by dynamical symmetries and dissipation](#)
J Tindall, C Sánchez Muñoz, B Bua et al.
- [Organisational hierarchy constructions with easy Kuramoto synchronisation](#)
Richard Taylor, Alexander C Kalloniatis and Keeley Hoek

Maximisation of synchronisability under low injection power

HISA-AKI TANAKA^{1(a)} , YOJI YABE¹, SOMEI SUGA¹, AKIRA KEIDA¹, KAI MAEDA¹, FUMITO MORI²
and HIROO SEKIYA³

¹ *The University of Electro-Communications - Tokyo 182-8585, Japan*

² *Kyushu University - Fukuoka 815-8540, Japan*

³ *Chiba University - Chiba 263-8522, Japan*

received 12 March 2024; accepted in final form 26 April 2024
published online 2 July 2024

Abstract – Synchronisability of limit cycle oscillators has been measured by the width of the synchronous frequency band, known as the Arnold tongue, concerning external forcing. We clarify a fundamental limit on maximizing this synchronisability within a specified extra low power budget, which underlies an important and ubiquitous problem in nonlinear science related to an efficient synchronisation of weakly forced nonlinear oscillators. In this letter, injection-locked Class-E oscillators are considered as a practical case study, and we systematically analyse their power consumption; our observations demonstrate the independence of power consumption in the oscillator from power consumption in the injection circuit and verify the dependency of power consumption in the oscillator solely on its oscillation frequency. These systematic observations, followed by the mathematical optimisation establish the existence of a fundamental limit on synchronisability, validated through systematic circuit simulations. The results offer insights into the energetics of synchronisation for a specific class of injection-locked oscillators.



Copyright © 2024 The author(s)

Published by the EPLA under the terms of the [Creative Commons Attribution 4.0 International License](https://creativecommons.org/licenses/by/4.0/) (CC BY). Further distribution of this work must maintain attribution to the author(s) and the published article's title, journal citation, and DOI.

Introduction. – Synchronisation (injection locking) of oscillators to an external forcing (injection signal) of widely different waveforms is often used to provide means for communicating among oscillators or linking between oscillators and their surrounding environment. In many branches of science and engineering, methods for efficient synchronisation, including explosive synchronisation [1], have been developed in recent years because synchronisability plays a prominent role in functioning of engineered systems and even in the social sciences [2]. The synchronisability is measured by the width of the Arnold tongue (cf. [3], p. 52); that is, the locking range (synchronous frequency band for the external forcing) in which the injection-locked state is maintained. During injection locking, the extra power is consumed through the injection of external forcing and this extra power is a matter of practical importance, for instance, in battery-limited electrical oscillators (*e.g.*, heart pacemakers). However, there seems to be insufficient knowledge on this extra power; as far as the authors know, even for the widely known van

der Pol oscillator, the extra power for maintaining injection locking has not been documented, despite of its long history. Motivated by recent studies conducted from a thermodynamic paradigm that clarify the thermodynamic uncertainty relation of the noisy van der Pol oscillator [4] as well as the energetics of the Stirling heat engine [5,6], coupled microscale phase oscillators [7], and a synchronising oscillator model [8], this study aims to provide an alternative, deterministic viewpoint on the energetics of injection locking, which is based on the observation from an existing practical electrical circuit.

Several recent studies have initially articulated the energetics of synchronisation from a stochastic thermodynamical viewpoint. For instance, [8] developed a general approach that unifies modelling and theoretical analysis for circadian systems. Notably, in their mathematical model and theory, the power consumption of the oscillator itself is independent from the extra power maintaining its synchronisation, which is hypothesised to relate to the amount of adenosine triphosphate (ATP) consumed throughout the oscillation cycles. Meanwhile, [7] first clarified the generic mechanism intrinsic to the mutually

^(a)E-mail: htanaka@uec.ac.jp (corresponding author)

coupled fluctuating phase oscillators with fixed circular trajectories. Interestingly, as in [8], the power consumption of the oscillator itself is separated and independent of the extra power for mutual synchronisation (cf. eq. (24) in [7]).

As opposed to these microscale systems in which stochastic thermodynamics becomes essential, how can the energetics of synchronisation be developed in deterministic systems? The van der Pol (vdP) oscillator is an example for such deterministic systems, for which van der Pol first observed injection locking [9]. The equation for the vdP oscillator, derived by van der Pol himself, is simple, but the analysis of its power consumption is not straightforward due to nonlinear resistance in the oscillator. As opposed to the vdP oscillator, Class-E amplifiers/oscillators, which have been widely used as power circuits [10–12], might be exotic to physicists. However, the Class-E oscillators are suitable for theoretical as well as numerical analysis of power consumption from the following reasons: i) Their power consumption analysis is straightforward because all the circuit elements are linear except for a single transistor; this transistor can be modelled as an ON/OFF switch in the working condition of this study. ii) Their nonlinear dynamics has been systematically analysed; a circuit experiment, numerical circuit simulations, and a phase reduction (to the phase equation below) have been confirmed to provide consistent results under various parameter settings [11,12]. This suitability for analysis motivated us to develop a case study concerning the energetics of synchronisation and a fundamental limit of synchronisability.

In this letter, we consider the extra power consumption required to maintain injection locking and address the following two problems that have been beyond the scope of the previous studies including [11,12].

Question 1: Can the power consumption of the oscillator itself and the extra power required for synchronisation be separated? Namely, is the extra power maintaining synchronisation given independently of the power consumption of the oscillator as it was in the energetics of [7,8]?

Question 2: Within a relatively small extra power budget for synchronisation, is it possible to maximise the synchronisability of the oscillator? Similarly, is it possible to minimise the extra injection power to achieve a certain level of synchronisability? Namely, does a fundamental limit of synchronisability exist for this particular example? The answers to these questions are given as *Answer 1* and *Answer 2*, respectively, at the end of this letter.

The rest of this letter is organised as follows. First, to answer the above questions, we provide a basic explanation of the circuit. Second, the power consumption in the oscillator itself and that in the injection circuit added to it are then systematically analysed through careful circuit simulations. Third, the simulation results demonstrate that these two power consumption sources can be treated separately in the injection-locked state; this en-

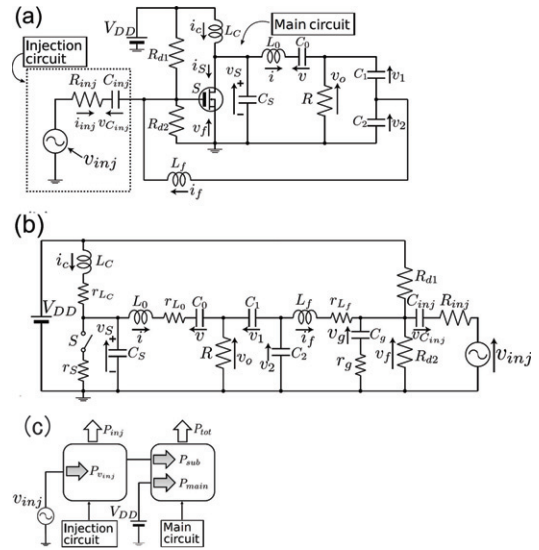


Fig. 1: The circuit system analysed in this study. (a) Injection-locked Class-E oscillator; the Class-E oscillator (main circuit) receives the injection signal (v_{inj}) through R_{inj} and C_{inj} . (b) Equivalent circuit; the MOSFET is effectively modelled as an ON/OFF switch. (c) Power flow; the shaded (blank) arrows indicate the power flowing into (out of) the circuit.

ables us to theoretically derive the optimal injection current waveform that maximises the locking range with the aid of the optimisation method in [13–15]. Thus, the fundamental limit of this synchronisability is proven to exist. Finally, we verify, through systematic, numerical analysis and experiment, that the theoretically determined optimal injection current is indeed optimal, which validates the existence of the fundamental limit.

Injection-locked Class-E oscillator. – We show, in fig. 1, the injection-locked Class-E oscillator [10–12], which is made up of a Class-E oscillator (the right part in fig. 1(a)) and an injection circuit (the left part in fig. 1(a)); first, the circuit elements of the Class-E oscillator are as follows: i) DC-supply voltage V_{DD} , ii) DC-feed inductance L_C , iii) switching device S ; the metal-oxide-semiconductor field-effect transistor (MOSFET) with r_S and gate threshold voltage V_{th} , iv) shunt capacitance C_S , v) series resonant circuit L_0 - C_0 - R , vi) voltage-dividing capacitances C_1 and C_2 , vii) feedback inductance L_f for phase shifting, and viii) resistors R_{d1} and R_{d2} , which are used to supply the bias voltage from the gate to the source of the MOSFET. These resistances are sufficiently large to keep the current through them negligible. In addition, for simplicity, we set $r_{L_C} = 0 \Omega$, $r_{L_0} = 0 \Omega$, and $r_{L_f} = 0 \Omega$, as in [12].

Second, the injection circuit is a simple RC circuit¹, as shown in fig. 1(a) and (b); we set $R_{inj} = 20 \text{ k}\Omega$ and $C_{inj} = 0.1 \mu\text{F}$, similar to the ones in [12], in this study.

¹This circuit configuration is similar to that of the membrane voltage clamping used to measure the membrane potential of neurons and cardiomyocytes in which R_{inj} is also large and C_{inj} is small [16].

Third, the circuit parameters in this study are tuned to almost the same values as those in [12], which were confirmed to satisfy the zero-voltage switching (ZVS) and zero-derivative switching (ZDS) conditions. These ZVS/ZDS conditions, which are essential for reducing the power consumption in the switching MOSFET effectively to zero, are detailed in sect. (A) of the appendix in the Supplemental Material `SupplementaryMaterial.pdf` (SM).

Power consumption in each part of the oscillator. – In what follows, first the power flow in the circuit is considered; we start from analysing each power consumption at the resistor R_{inj} in the injection circuit in fig. 1(a) and those at the five resistors R , r_g , R_{d1} , R_{d2} , and r_S in the main circuit shown in fig. 1(b) are obtained subsequently. Next, we clarify that the power consumption in the main circuit is dependent upon the synchronised oscillation frequency under injection locking, where the oscillation frequency is synchronised to the frequency of the injection signal. To this end, we observe that two metrics—the injection power (P_{inj} in eq. (3)) and total power consumption in the main circuit (P_{tot})—are independent and separate.

To begin with, we denote T ($= 2\pi/\Omega$) s and Ω rad/s as the injection-locked oscillation period and the frequency of the injection signal, respectively. In addition, ω is the natural frequency of the free-running oscillator (without injection signal) and the frequency detuning $\Delta\omega \equiv \omega - \Omega$ is the difference between them. The circuit equation, which has been provided in [10], is obtained from standard nodal analysis for the equivalent circuit illustrated in fig. 1(b); all the circuit parameter values are listed in table B.1 in sect. (B) in the SM, which satisfy the ZVS/ZDS conditions. For the numerical integration of the circuit equation, we employed the fourth-order Runge-Kutta method with time step $\Delta t = 2\pi/(2000\omega)$ ($\simeq 3.1$ ns) in this study. The source code in C used to define the circuit equation and the circuit parameters is provided in the supplementary file `function.c`.

We start by considering the power flow in the main circuit (the right part in fig. 1(c)). Hereafter, we use the abbreviation: $\langle\langle \cdot \rangle\rangle \equiv (2\pi)^{-1} \int_0^{2\pi} \cdot d\theta$ with $\theta \equiv \Omega t$, and we define the norm by $\|f\|_2 \equiv \langle\langle f^2(\theta) \rangle\rangle^{\frac{1}{2}}$ for any function f , with $\|f\|_2 < \infty$. Then, in the injection-locked states, the power P_{main} supplied from the DC voltage source (V_{DD}) is

$$P_{main} = \frac{1}{T} \int_0^T i_c(\Omega t) V_{DD} dt = \langle\langle i_c(\theta) V_{DD} \rangle\rangle.$$

In contrast, the power consumption P_{out} (output power) at the resistor R is

$$P_{out} = \frac{1}{T} \int_0^T R^{-1} v_o^2(\Omega t) dt = R^{-1} \langle\langle v_o^2(\theta) \rangle\rangle.$$

Power dissipation in other resistors r_g , R_{d1} , R_{d2} , and r_S is obtained similarly. Furthermore, the power P_{sub} supplied

from the injection circuit to the main circuit is

$$P_{sub} = \langle\langle i_{inj}(\theta) v_f(\theta) \rangle\rangle. \quad (1)$$

Let P_{tot} be the sum of the power dissipated by the above five resistors in the main circuit, which is equal to the power supplied to the main circuit ($P_{main} + P_{sub}$). Then, $P_{tot} = P_{main} + P_{sub}$ always holds; note that the values of P_{tot} , P_{main} , and P_{sub} obtained from numerical circuit simulations in table B.2 satisfy the relation $P_{tot} = P_{main} + P_{sub}$ with high accuracy, which verifies the validity and correctness of the circuit simulations.

Next, we consider the remaining power flow in the injection circuit (the left part in fig. 1(c)); i) in the injection-locked state, the power $P_{v_{inj}}$ supplied from the injection voltage v_{inj} to the injection circuit is

$$P_{v_{inj}} = \langle\langle i_{inj}(\theta) v_{inj}(\theta) \rangle\rangle. \quad (2)$$

ii) Similarly, the power consumption P_{inj} at the resistor R_{inj} is

$$P_{inj} = \langle\langle i_{inj}^2(\theta) R_{inj} \rangle\rangle. \quad (3)$$

iii) P_{sub} , which amounts to the power supply $P_{v_{inj}}$ minus the power consumption P_{inj} in the injection circuit, is supplied to the main circuit. Then $P_{sub} = P_{v_{inj}} - P_{inj}$ always holds; the values of $P_{v_{inj}}$, P_{inj} , and P_{sub} obtained from numerical circuit simulations in tables B.2 and B.3 of the SM satisfy $P_{sub} = P_{v_{inj}} - P_{inj}$ with high accuracy. Figure 1(c) summarises the power flow in the circuit described above.

Finally, as shown in fig. 2 (and fig. B.2 in the SM), the input frequency Ω dependence of the power consumption in the circuit is analysed using numerical circuit simulations; we vary Ω centered at $\Omega/2\pi = \omega/2\pi = 1.979$ MHz, *i.e.*, $\Delta\omega = 0$. For each value of Ω , by controlling the magnitude of i_{inj} , the power consumption P_{inj} in the injection circuit is set to a constant value; in eq. (3) with $R_{inj} = 20$ k Ω , by setting $\langle\langle i_{inj}^2 \rangle\rangle = 4.5 \times 10^{-8}$, $P_{inj} = 9.0 \times 10^{-4}$ W ($= 4.5 \times 10^{-8}$ A $^2 \times 20.0 \times 10^3$ Ω) always holds. Another essential source code in sect. (C) for generating data in fig. 2 and fig. B.2 is provided in the supplementary file `main.c`. In this study, we use the injected current i_{inj} for a sine wave, a square wave, a broad bipolar pulse wave, and the optimal waveform (eventually obtained as eq. (13)) satisfying $\langle\langle i_{inj}^2 \rangle\rangle = 4.5 \times 10^{-8}$. The corresponding waveforms are shown in fig. B.1 in sect. (B) in the SM. The choice of somewhat broad pulse (duty ratio 20 (%)) is due to the following reasons: i) The magnitude of the injected current needs to be reduced to protect the circuit in practical circuit environments, and ii) the same broad bipolar pulse has been used in the real circuit experiments of [12]. The power consumption of each resistor in the main circuit for each waveform for $\Delta\omega = 0$ is shown in table B.2 of the appendix in the SM; for the respective injection currents of sine, square, pulse, and optimum waveforms, the power consumption in R , r_g , R_{d1} , R_{d2} , r_S and its sum P_{tot} , power supply P_{main} , and

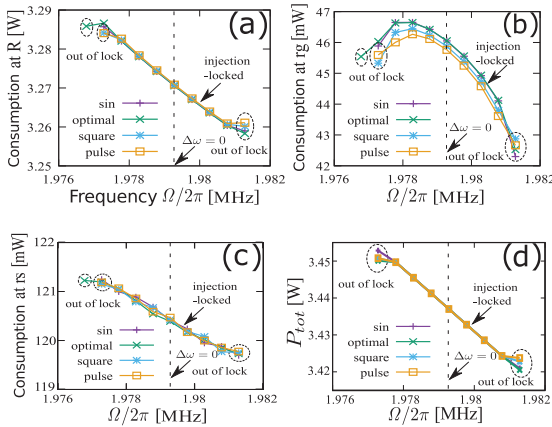


Fig. 2: The oscillation frequency dependence of the power consumption in each resistor: (a) R , (b) r_g , (c) r_s , and its sum (d) P_{tot} ; (a) is the major part of (d), while both (b) and (c) are minor parts of (d). “Injection-locked” and “out of lock” surrounded by dotted lines indicate injection-locked and asynchronous states, respectively. In addition, +, ×, *, and □ denote the data of sinusoidal, optimal, square, and pulse wave injection current i_{inj} , as shown in the SM, in figs. B.1 (a), (b), (c), and (d), respectively. Note: in the injection-locked state, the power consumption (averaged over $T (= 2\pi/\Omega)$) does not depend on the timing of observation because the system is purely periodic in T . On the other hand, in the out of lock (asynchronous) condition, the system exhibits intermittent phase slips (cf. [3], pp. 53, 54, 81–83) and is no longer purely periodic, which results in a spread in the time-dependent values of the power consumptions, as observed in the above graphs.

P_{sub} supplied from the injection circuit to the main circuit, and $P_{v_{inj}}$ supplied by v_{inj} are listed. Furthermore, fig. 2 (and fig. B.2 in the SM) compare, respectively, the power consumption of each resistor, P_{sub} and $P_{v_{inj}}$ when the value of Ω is varied in and out of the locking range, centered at $\Delta\omega = 0$. Note that, for each i_{inj} , the injection locking is directly observed by comparing the frequency of the oscillator and the (tunable) frequency Ω of i_{inj} ; the locking range is uniquely and accurately obtained for each given magnitude of i_{inj} . Although the power consumption of R_{d1} and that of R_{d2} are omitted in fig. 2, they are all in the order of μW as shown in table B.2 in the SM; they show the same input frequency dependence as the power consumption of other resistors.

Observations of total power consumption. – While scrutinising the results of tables B.2 and B.3 and fig. 2 (and fig. B.2 in the SM), we made the following observations (O1) and (O2) on the supposition that the following conditions (i), (ii), (iii) are met: i) weak forcing (*i.e.*, low injection power P_{inj}), ii) $R_{inj}C_{inj} \ll (\Omega/2\pi)^{-1}$, and iii) the ZVS/ZDS conditions (*i.e.*, basic circuit design constraints mentioned above).

(O1) For given various injection currents i_{inj} under the same low injection power $P_{inj} (= 9.0 \times 10^{-4} \text{ W}$ above), the power consumption of each resistor R, r_g, R_{d1}, R_{d2} , and

r_s in the main circuit, and their sum P_{tot} do not show significant difference for all waveforms of i_{inj} as long as the circuit is injection-locked, as shown in fig. 2.

(O2) The total power consumption P_{tot} described above is specific to the oscillator itself, which depends only on the oscillation frequency, independent of whether there is injection locking or not. In addition, its oscillation frequency dependence shows only a relatively small change for this particular Class-E oscillator; see fig. C.1 and details in sect. (C) of the appendix in the SM.

Viewed from the general theory of limit cycle oscillators under weak forcings [17,18], the above (O1) and (O2) seem natural and consistent with it; the oscillation waveform (*i.e.*, oscillation state) of a limit cycle oscillator synchronised to a weak forcing (*i.e.*, a weak perturbation $f(\Omega t)$ in $\Gamma(\phi)$ below of the order $O(\varepsilon)$) will be only slightly deformed by at most $O(\varepsilon)$ compared to its original oscillation waveform without forcings. Then, the observations (O1) and (O2) can be summarised as follows: i) The power consumption P_{tot} of the oscillator itself (the main circuit) in the injection-locked state shows only a slight change from that of the oscillator without forcing. ii) This slight change of P_{tot} is attributed to the oscillation frequency dependence of the power consumption in the oscillator itself. This is because the main circuit, which oscillates at a frequency different from its natural frequency under injection locking, slightly changes its power consumption depending on its oscillation frequency (for details, see sect. (C) of the appendix in the SM).

From the above i) and ii), under a weak forcing, the power consumption of the oscillator itself (P_{tot} in fig. 1(c)) and that of the injection circuit (P_{inj} in fig. 1(c)), which is additionally required for the injection locking, are given independently; for any (small) P_{inj} , P_{tot} depends only on the oscillation frequency, and it is not influenced by the value of P_{inj} nor by the waveforms of i_{inj} . Therefore, it is reasonable to analyse the influence of the input waveform i_{inj} on its locking range only by setting the power consumption P_{inj} to a specific (small) value.

Relationship between injection current and voltage. – To analyse the input waveform dependence of the locking range, it is useful to obtain an equation relating the injection current i_{inj} and injection voltage v_{inj} in the injection circuit. First, the circuit equation for the injection circuit in fig. 1(a) is

$$v_{inj}(t) = R_{inj}i_{inj}(t) + C_{inj}^{-1} \int_0^t i_{inj}(t') dt' + v_f(t). \quad (4)$$

In eq. (4), of interest is the injection-locked state at the input frequency $\Omega/2\pi$ (as shown in fig. 1(a)); replacing t in eq. (4) with $\theta \equiv \Omega t$, the periodic solutions of $i_{inj}(\theta)$, $v_{inj}(\theta)$, and $v_f(\theta)$ in Fourier series with period 2π are obtained using the harmonic balance method. See sect. (D) of the appendix in the SM for details. As a result, we have the following concise relation between i_{inj} and v_{inj} :

$$i_{inj}(\theta) = R_{inj}^{-1}[v_{inj}(\theta) - \bar{v}_{C_{inj}} - v_f(\theta)], \quad (5)$$

where $\bar{v}_{C_{inj}}$ is a time-independent constant². Note that the condition $R_{inj}C_{inj} \gg (\Omega/2\pi)^{-1}$, as shown in sect. (D) of the appendix in the SM, is naturally satisfied in this study, which makes the derivation of eq. (5) simpler.

As a result of eq. (5), when the constant part of i_{inj} is set to 0, *i.e.*, $\langle\langle i_{inj}(\theta) \rangle\rangle = 0$, the following relation holds: $\langle\langle v_{inj} \rangle\rangle - \bar{v}_{C_{inj}} - \langle\langle v_f \rangle\rangle = 0$. This implies that $\bar{v}_{C_{inj}}$ ($= \langle\langle v_f \rangle\rangle - \langle\langle v_{inj} \rangle\rangle$) is a constant voltage determined by the difference in the constant parts of v_f and v_{inj} under synchronisation, which is naturally consistent with the insight obtained from the injection circuit of fig. 1(a).

Proof of fundamental limit by optimal injection current. – Having observed that the two metrics P_{inj} and P_{tot} are independent (and hence P_{tot} does not appear below), and having determined the relation (5) between i_{inj} and v_{inj} during injection locking, we will now prove the fundamental limit of synchronisability by directly constructing the optimal input waveform of i_{inj} for a given P_{inj} in the following steps (i), (ii), (iii)).

i) As the first step towards this objective, we introduce the phase reduction method here. In nonlinear oscillators, including Class-E oscillators in which a weak external forcing $f(\Omega t)$ is injected, the long-term dynamics of the injection-locking process can be reduced to the following phase eq. (cf. [13,17,18]): $d\phi/dt = \Delta\omega + \Gamma(\phi)$, where $\Gamma(\phi) = \langle\langle Z(\theta + \phi)f(\theta) \rangle\rangle$, with ϕ representing the phase difference between the oscillator and the external signal, and $\Delta\omega \equiv \omega - \Omega$ denotes the frequency difference between the oscillator and external signal. $\Gamma(\phi)$ is a periodic function with period 2π and is called a phase coupling function. The phase sensitivity function $Z(\theta)$ is a 2π -periodic function intrinsic to the oscillator that indicates the influence (sensitivity) of the external signal on the oscillation phase.

It is known that this Z can be obtained using various methods [18]. Specifically, in the Class-E oscillator shown in fig. 1(a), both $i_{inj}(\Omega t)$ and $v_{inj}(\Omega t)$ of the injection circuit can be selected as the external forcing $f(\Omega t)$ above, and we write the phase sensitivity function corresponding to i_{inj} and v_{inj} as $Z_I(\theta)$ and $Z_V(\theta)$, respectively. In recent experimental studies of Class-E oscillators [11,12], v_{inj} has been treated as the external forcing, simply because v_{inj} is relatively easily controlled in circuit experiments (compared to controlling i_{inj}). Hence, [12] introduces the constraint of a given (relatively small) mean square of the input voltage $\langle\langle v_{inj}^2 \rangle\rangle$ (in eq. (8)). However, this constraint does not correspond to the power consumption of the circuit P_{inj} (and P_{tot}) since, apparently, $\langle\langle v_{inj}^2 \rangle\rangle \neq \langle\langle i_{inj}^2 R_{inj} \rangle\rangle (= P_{inj})$.

ii) As the next step toward the fundamental limit, we need to consider i_{inj} as an external forcing. Now, the objective is to find the optimal injection current i_{opt} that maximises the locking range among feasible i_{inj} wave-

forms. According to the previous observations (O1) and (O2), if the power consumption of the input circuit P_{inj} ($= \langle\langle i_{inj}^2 R_{inj} \rangle\rangle$) is constrained to a small, constant value (as in eq. (6) below), the total power consumption P_{tot} of the main circuit under synchronisation is found to be independent of the waveform of i_{inj} . Thus, the optimisation problem of maximising the locking range ($\equiv \mathcal{L}[i_{inj}]$ in eq. (9) below), given as a functional of i_{inj} , makes sense and is well defined under the following constraints 1 and 2 for i_{inj} .

Constraint 1: P_{inj} is a given constant ($= MR_{inj}$), *i.e.*,

$$\|i_{inj}\|_2 \left(\equiv \langle\langle i_{inj}^2(\theta) \rangle\rangle^{\frac{1}{2}} \right) = M, \quad (6)$$

Constraint 2: $\langle\langle i_{inj}(\theta) \rangle\rangle = 0$, (7)

as opposed to the ones initially assumed in [12]:

$$\langle\langle v_{inj}^2(\theta) \rangle\rangle^{\frac{1}{2}} = M, \quad \langle\langle v_{inj}(\theta) \rangle\rangle = 0. \quad (8)$$

Constraint 2, often called the charge balance constraint, is required to protect the circuit, in which the net injected charge should be zero. On the other hand, the objective function $\mathcal{L}[i_{inj}]$ (functional of i_{inj}), *i.e.*, the locking range, is given by the difference between the minimum value $\Gamma(\phi_{min})$ and the maximum value $\Gamma(\phi_{max})$ of $\Gamma(\phi)$ ($= \langle\langle Z(\theta + \phi)i_{inj}(\theta) \rangle\rangle$) as determined for any feasible i_{inj} [12]:

$$\begin{aligned} \mathcal{L}[i_{inj}] &= \Gamma(\phi_{min}) - \Gamma(\phi_{max}) \\ &= \langle\langle [Z_I(\theta + \phi_{min}) - Z_I(\theta + \phi_{max})]i_{inj}(\theta) \rangle\rangle, \end{aligned} \quad (9)$$

where ϕ_{max} and ϕ_{min} satisfy the conditions that $\Delta\omega_{max} + \Gamma(\phi_{max}) = 0$ and $\Delta\omega_{min} + \Gamma(\phi_{min}) = 0$, and $\Delta\omega_{max}$ and $\Delta\omega_{min}$ correspond to the rightmost maximum and leftmost minimum of the locking range for i_{inj} , respectively (cf. [12]). Hereafter, we denote $\phi_{min} - \phi_{max} \equiv \Delta\phi$.

iii) As the final step, we introduce an additional parameter μ and define a functional $\mathcal{J}[i_{inj}; \mu]$ for maximising the locking range $\mathcal{L}[i_{inj}]$ under constraints 1 and 2:

$$\mathcal{J}[i_{inj}; \mu] \equiv \mathcal{L}[i_{inj}] + \mu [\langle\langle i_{inj}(\theta) \rangle\rangle - 0] = \langle\langle i_{inj}g \rangle\rangle, \quad (10a)$$

$$\text{with } g(\theta) \equiv Z_I(\theta + \Delta\phi) - Z_I(\theta) + \mu. \quad (10b)$$

We note that this method for embedding the constraint 2 (eq. (7)) into the functional \mathcal{J} through the additional parameter μ was first introduced in [13] and further developed in [19]; it is useful for solving a certain (convex) optimisation problem via the Hölder/Cauchy-Schwarz inequality. Note that the constraint 1 (eq. (6)) is also embedded in the process of optimisation (12) below, and the parameters μ and $\Delta\phi$ are finally determined by solving eqs. (7), (13) for μ and $\Delta\phi$.

Thus, finding the optimal injection current i_{opt} is reduced to solving the following optimisation problem:

$$\begin{aligned} &\text{maximise } \mathcal{J}[i_{inj}; \mu], \\ &\text{subject to } \langle\langle i_{inj} \rangle\rangle = 0, \quad \|i_{inj}\|_2 = M, \end{aligned} \quad (11)$$

²The relation between i_{inj} and v_{inj} in eq. (5) can also be obtained by analytically solving the initial value problem for eq. (4) and setting $t \rightarrow \infty$, but its calculation is lengthy and omitted here.

which can be solved with the calculus of variations (as the Euler-Lagrange equation), leading to the same result as that we obtain below (cf. [14,15,20]). However, we resort to the following direct approach from eq. (10), which uses only inequalities, due to its simplicity and clarity:

$$\begin{aligned} \mathcal{J}[i_{inj}; \mu] &= \mathcal{J}[i_{inj}; \mu_{opt}] = \langle\langle i_{inj}g \rangle\rangle \leq \langle\langle |i_{inj}g| \rangle\rangle \equiv \|i_{inj}g\|_1 \\ &\leq \|i_{inj}\|_2 \|g\|_2 = M \|g\|_2. \end{aligned} \quad (12)$$

Here the equality condition: $i_{inj}(\theta) \sim g(\theta)$ of the Cauchy-Schwarz inequality $\|i_{inj}g\|_1 \leq \|i_{inj}\|_2 \|g\|_2$ is essential. By $i_{inj} \sim g$, the i_{opt} realising the upper bound in eq. (13) must be of the following form (if it exists):

$$i_{opt}(\theta) = M g_{opt}(\theta) / \|g_{opt}\|_2, \quad (13)$$

and this i_{opt} makes all “ \leq ” as “ $=$ ” in eq. (13), which implies that i_{opt} is the maximiser of $\mathcal{L}[i_{inj}]$ under constraints (6) and (7). Finally, by substituting eq. (13) into (6) and (7), $\mu_{opt} = 0$ and $\Delta\phi_{opt} = \pi$ are uniquely determined for a given $Z_I(\theta)$ in fig. 3(a), following the careful numerical analysis in [13], sect. 6, which implies that i_{opt} does exist. We note that the solution $\Delta\phi_{opt} = \pi$ is proven to always exist (cf. [13], below Theorem 1, p. 6; and the “generic solution” in [14], p. 2). Thus, after plugging $(\Delta\phi, \mu) = (\Delta\phi_{opt}, \mu_{opt}) = (\pi, 0)$ in eq. (10b) we obtain $g_{opt}(\theta) = Z_I(\theta + \pi) - Z_I(\theta)$, which implies that i_{opt} in eq. (13) together with the above g_{opt} is the unique maximiser of $\mathcal{J}[i_{inj}; \mu]$; i_{opt} maximises the locking range \mathcal{L} under constraints (6) and (7). In addition, the corresponding injection voltage $v_{opt}(\theta)$ (fig. 3(b), green graph), which yields i_{opt} in eq. (13), is uniquely determined by the relation in eq. (5) (with the numerically obtained $\bar{v}_{C_{inj}}$ and $v_f(\theta)$ in eq. (5), as explained below).

Finally, through numerical circuit simulations, we verify that the theoretically obtained i_{opt} in eq. (13) is indeed realised by setting v_{inj} as the theoretically obtained v_{opt} in the injection circuit in the following manner: First, the circuit simulations in this study employ the switch model in fig. 1(b); the timing at which the MOSFET enters the “ON” state is set to $\theta = 0$, and the timing at which the MOSFET enters the “OFF” state is set to $\theta = \pi$, for simplicity. This makes the phase θ in eq. (5) and $Z_I(\theta)$ is uniquely fixed on the θ coordinate; on this coordinate, we observe that under injection locking, i_{opt} , v_{opt} , and v_f , as shown in fig. 3(b) via circuit simulations, satisfy eq. (5) with high accuracy. Next, we compare this numerically obtained v_{opt} with the above theoretically obtained one. The result shows that they are indistinguishable on the graph in fig. 3(b), which implies that i_{opt} is indeed realised in the circuit by injecting v_{opt} .

Verification of optimality. – The optimality of the injection current i_{opt} and the corresponding v_{opt} obtained in the previous section is validated in the following two ways. First, to verify that the optimal injection current i_{opt} indeed maximises the locking range, the value of the locking range for i_{opt} is compared with that of the locking

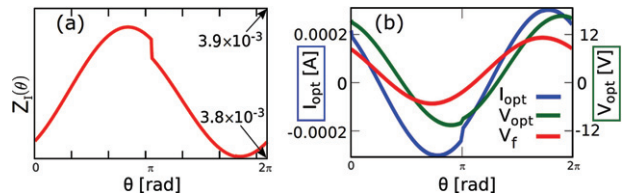


Fig. 3: Verification of the validity of i_{opt} for injected v_{opt} . (a) Phase sensitivity function $Z_I(\theta)$ for injection current i_{inj} . (b) Observed injection current i_{opt} and corresponding injection voltage v_{opt} and v_f . These are obtained through the numerical circuit simulations, and eq. (5) is verified to be satisfied by them.

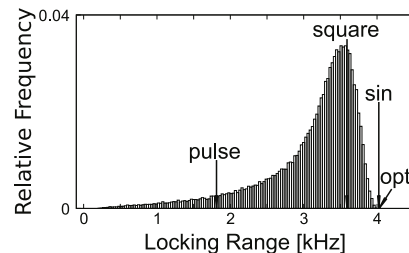


Fig. 4: Distribution of locking ranges for 10^5 randomly generated injected currents of i_{inj} . Pulse, square, sin, and opt in the figure correspond to the cases in which i_{inj} has (broad bipolar) pulse, square, sinusoidal, and optimal waveforms in fig. B.1, respectively. Their locking ranges are 1.811, 3.590, 4.024 and 4.028 kHz, respectively. Note that the optimal waveform (opt) significantly outperforms the pulse and square waveforms, while it outperforms the sinusoidal waveform only slightly.

range for the randomly generated, injected current waveform; specifically, for i_{inj} (that satisfies the constraints (6) and (7)) of 100000 fifth-order Fourier series³ with Fourier coefficients generated by uniform random numbers, the distribution of the locking ranges is obtained from the phase equation (fig. 4). As can be seen in fig. 4, the locking range for i_{opt} is wider than that for any other input waveform, although the locking range for i_{opt} and that for the sinusoidal i_{inj} are quite close.

Second, the consistency between i_{opt} in this study and the previous result in [12] is further verified; the optimal injection voltage v_{opt}^* , previously obtained in [12] (from $v_{opt}(\theta) = M g_{opt}(\theta) / \|g_{opt}\|_2$, similar to eq. (13)) for the external forcing v_{inj} , has almost the same shape as that of i_{opt} obtained in this study, because Z_I in this study and Z_V in [12] have almost the same shape. Namely, the optimality of v_{opt}^* in [12] under constraint (8) implies the optimality of i_{opt} under constraints (6) and (7). For more detail, see section (E) in the SM.

³Note that the fifth-order Fourier series for i_{inj} are sufficient for this analysis, because Z_I in this study has small magnitude in their higher harmonics, which implies higher harmonics in the injection current i_{inj} does not affect Γ in the phase equation: $d\phi/dt = \Delta\omega + \Gamma(\phi)$.

Discussion. – Although this study is conducted for the injection-locked Class-E oscillator for which power consumption analysis is easily carried out, the obtained framework can be useful for analysing other injection-locked oscillators; for example, the injection-locked CMOS ring oscillators [21] as well as the vdP oscillator [9], with a similar injection circuit in this study. This is because observations (O1) and (O2) are expected for those oscillators as general properties of synchronous oscillators with weak forcings [17,18], which implies such a specific class of injection-locked oscillators is amenable to the framework of this study. However, we need to be cautious in using our method for the following technical reasons; firstly, the power consumption in the injection circuit needs to be reliably estimated (or controlled to be a small value), which implies a relatively simple injection circuit (such as the linear circuit in this study) would be a reasonable choice. Secondly, the separability of the (low) injection power P_{inj} and the total power consumption P_{tot} in the oscillator needs to be verified (as in (O1)), which requires a reliable estimation of P_{tot} including power consumptions in the nonlinear elements; the transistor working as the ON/OFF switch in this study would be an ideal instance. Finally, as a future study, it is theoretically as well as practically interesting to consider the implications of the pioneering framework in [22] for our particular circuits, where the feature size of the transistors is scaled below several nm. In addition, an extension toward energy propagation on networks [23,24] from our framework is open for future study.

Conclusion. – This study verifies that the power consumption of the Class-E oscillator and the extra power required in the injection circuit can be separated, and shows that the locking range can be maximised under the constraint of a weak power consumption of the injection circuit. Specifically, the following findings were obtained respectively for *Question 1* and *Question 2* raised at the beginning of this letter, which characterise the fundamental limit of synchronisability for this particular oscillator.

Answer 1: In the injection-locked Class-E oscillator of this study, the power consumption of the oscillator itself and the extra power consumption in the injection circuit are independent and can be treated separately as far as the injection locking is maintained.

Answer 2: Under the condition: $(R_{inj}C_{inj})^{-1} \ll \Omega/2\pi$, for a given low injection power, the locking range can be maximised by designing the optimal injection current i_{opt} (of eq. (13)), obtained through the optimal injection voltage v_{opt} due to the one-to-one correspondence between i_{inj} and v_{inj} according to eq. (5). It is also immediately obtained from eq. (12) that for this i_{opt} , under a given locking range ($= \mathcal{L}[i_{inj}] = \mathcal{J}[i_{inj}]$ of eq. (12) since i_{opt} satisfies $\langle\langle i_{opt} \rangle\rangle = 0$), the injected power ($\sim M$ of eq. (12)) is minimised. This is because all “ \leq ” become “ $=$ ” in eq. (12) which implies i_{opt} minimises M .

This work was supported in part by JSPS KAKENHI (JP24K03008). FM acknowledges JSPS KAKENHI (JP22K03453) for financial support.

Data availability statement: All data that support the findings of this study are included within the article (and any supplementary files).

REFERENCES

- [1] BAYANI A., JAFARI S., AZARNOUSH H., NAZARIMEHR F., BOCCALETTI S. and PERC M., *Chaos, Solitons Fractals*, **169** (2023) 113243.
- [2] KOVALENKO K., DAI X., ALFARO-BITTNER K., RAIGORODSKII A. M., PERC M. and BOCCALETTI S., *Phys. Rev. Lett.*, **127** (2021) 258301.
- [3] PIKOVSKY A., ROSENBLUM M. and KURTHS J., *Synchronization: A Universal Concept in Nonlinear Sciences* (Cambridge University Press, Cambridge, England) 2003.
- [4] HASEGAWA Y. and VU T. V., *Phys. Rev. E*, **99** (2019) 062126.
- [5] KADA H., HOJYO H. and TOKUDA I. T., *Nonlinear Theory Appl. IEICE*, **5** (2014) 466.
- [6] IZUMIDA Y., *EPL*, **121** (2018) 50004.
- [7] IZUMIDA Y., KORI H. and SEIFERT U., *Phys. Rev. E*, **94** (2016) 052221.
- [8] ZHANG D., CAO Y., OUYANG Q. and TU Y., *Nat. Phys.*, **16** (2020) 95.
- [9] VAN DER POL B. and VAN DER MARK J., *Nature*, **120** (1927) 363.
- [10] KAZIMIERCZUK M. K., KRIZHANOVSKI V. G., RAS-SOKHINA J. V. and CHERNOV D. V., *IEEE Trans. Circuits Syst. I*, **53** (2006) 1214.
- [11] NAGASHIMA T., WEI X., TANAKA H.-A. and SEKIYA H., *IEEE Trans. Circuits Syst. I*, **61** (2014) 2904.
- [12] YABE Y., TANAKA H.-A., SEKIYA H., NAKAGAWA M., MORI F., UTSUNOMIYA K. and KEIDA A., *IEEE Trans. Circuits Syst. I*, **67** (2020) 1762.
- [13] TANAKA H.-A., *Physica D*, **288** (2014) 1.
- [14] HARADA T., TANAKA H.-A., HANKINS M. J. and KISS I. Z., *Phys. Rev. Lett.*, **105** (2010) 088301.
- [15] ZLOTNIK A., CHEN Y., KISS I. Z., TANAKA H.-A. and LI J.-S., *Phys. Rev. Lett.*, **111** (2013) 024102.
- [16] WILSON W. A. and GOLDNER M. M., *J. Neurobiol.*, **6** (1975) 411.
- [17] KURAMOTO Y., *Chemical Oscillations, Waves, and Turbulence* (Springer, Berlin) 1984.
- [18] KATO Y., YAMAMOTO N. and NAKAO H., *Phys. Rev. Res.*, **1** (2019) 033012.
- [19] TANAKA H.-A., NAKAGAWA M. and OOHAMA Y., *Entropy*, **21** (2019) 549.
- [20] HATA S., ARAI K., GALÁN R. F. and NAKAO H., *Phys. Rev. E*, **84** (2011) 016229.
- [21] RAZAVI B., *IEEE J. Solid-State Circuits*, **39** (2004) 1415.
- [22] FREITAS N., DELVENNE J.-C. and ESPOSITO M., *Phys. Rev. X*, **11** (2021) 031064.
- [23] JI P., YE J., MU Y., LIN W., TIAN Y., HENS C., PERC M., TANG Y., SUN J. and KURTHS J., *Phys. Rep.*, **1017** (2023) 1.
- [24] MAJHI S., PERC M. and GHOSH D., *J. R. Soc. Interface*, **19** (2022) 20220043.